Materials Science & Engineering A 646 (2015) 306–314

Contents lists available at ScienceDirect

Materials Science & Engineering A

journal homepage: www.elsevier.com/locate/msea

Aluminum powder size and microstructure effects on properties of boron nitride reinforced aluminum matrix composites fabricated by semi-solid powder metallurgy

Cunguang Chen [a], Leichen Guo [b], Ji Luo [a], Junjie Hao [a], Zhimeng Guo [a,*], Alex A. Volinsky [c]

[a] Institute for Advanced Materials and Technology, University of Science and Technology Beijing, Beijing 100083, PR China
[b] School of Engineering, Rensselaer Polytechnic Institute, Troy, NY 12183, USA
[c] Department of Mechanical Engineering, University of South Florida, Tampa, FL 33620, USA

ARTICLE INFO

Article history:
Received 13 July 2015
Received in revised form
22 August 2015
Accepted 24 August 2015
Available online 28 August 2015

Keywords:
Powder metallurgy
h-BN
Al matrix composite
Semi-solid processing

ABSTRACT

Al matrix composite reinforced by hexagonal boron nitride (h-BN) with nearly full densification was successfully fabricated by the semi-solid powder metallurgy technique. The h-BN/Al composites were synthesized with elemental pure Al powder size of d_{50}=35, 12 and 2 μm. The powder morphology and the structural characteristics of the composites were analyzed using X-ray diffraction, scanning and transmission electron microscopy. The density, Brinell hardness and compressive behavior of the samples were characterized. Density measurement of the Al composites revealed that the composite densification can be effectively promoted by plenty of embedded liquid phase under pressure. Composites prepared using Al powder with varying granularity showed different grain characteristics, and in situ recrystallization occurred inside the original grains with 35 μm Al powder. A sharp interface consisting of Al/Al_2O_3/h-BN was present in the composites. Both the compressive strength and the fracture strain of the investigated composites increased with the decrease of the Al powder size, along with the Brinell hardness. The composite with 2 μm Al powder exhibited the highest relative density (99.3%), Brinell harness (HB 128), compressive strength (763 MPa) and fracture strain (0.299).

1. Introduction

Al alloys and Al matrix composites produced by powder metallurgy (PM) have been receiving more attention than conventional melting-casting methods in aerospace, military and car industries, due to the improved physical, chemical and mechanical properties [1–3]. The large surface area of fine Al or Al alloy powders makes it possible to introduce naturally formed ultrathin and dense surface oxides, which cannot be reduced to Al [4]. The oxide film will hinder metallurgical bonding between the powder particles and cause the formation of voids during the sintering process of the green compacts [5]. Thus, it is difficult to obtain fully dense Al alloys and Al matrix composites with clean and sharp interfaces. In particular, low wettability and inhomogeneous distribution of ceramic reinforcements are the main issues in the Al matrix composites (AMCs) preparation. Therefore, the worldwide effort has been to develop a short pressing-sintering process to obtain high performance Al alloys and Al matrix composites, similar to the iron-based products processing. To fabricate fully dense Al-based materials by powder metallurgy, conventional consolidation methods have been commonly used, including sintering and hot isostatic pressing (HIP) [6], extrusion [7], forging [8] and rolling [9]. These processes need large amounts of energy and have higher operating requirements. In recent years the semi-solid powder forging has been attracting an increased interest due to short processing and low energy consumption. Actually, the semi-solid powder forging is one kind of semi-solid powder processing [10], which combines the benefits of the semi-solid forming and powder metallurgy. In general, the semi-solid powder forging involves four basic steps: powder preparation, powder pre-compaction, heating and semi-solid forging. This technique has been successfully applied in processing alloy materials, such as Al6061 [10] and Al–Ti [11], and composite materials, including Al–SiC [12] and Al-CNT [13].

Hexagonal boron nitride (h-BN), also known as white graphite, has lamellar crystalline structure with excellent lubricating properties. Accordingly, h-BN is an important solid lubricant with numerous industrial applications. Moreover, it has key properties, such as high thermal conductivity, low thermal expansion, good thermal shock resistance, high electrical resistance, low dielectric constant and microwave transparency [14]. Additionally, h-BN has

* Corresponding author.
E-mail addresses: zmguo@ustb.edu.cn (Z. Guo), volinsky@usf.edu (A.A. Volinsky).

http://dx.doi.org/10.1016/j.msea.2015.08.081
0921-5093/

good neutron absorption ability and high workability. The h-BN is a light weight ceramic material with low theoretical density of only 2.25 g cm^{-3}, which is less dense than pure aluminum (2.7 g cm^{-3}) and common strengthening particles, such as SiC (3.22 g cm^{-3}) and Al_2O_3 (3.97 g cm^{-3}). Due to h-BN outstanding properties, it has been extensively investigated as ceramic dispersant in metals [15–19]. Hence, there is an important possible application of h-BN as the dispersed phase in AMCs with light weight and high performance. However, there still exists the crucial problem of poor bonding between the h-BN and the Al matrix. To overcome this problem, several manufacturing methods have been proposed, mainly including high energy ball milling [15] and pressureless infiltration [18].

In this investigation, elemental pure aluminum and copper powder were utilized to prepare h-BN reinforced Al–Cu matrix composites by the semi-solid powder forging. The aim of this paper was to evaluate the effects of aluminum powder size on the microstructure and mechanical properties of the as-forged h-BN/Al–Cu composites.

2. Experimental procedure

2.1. Material

Three different kinds of commercially available gas atomized Al powders with $d_{50}=35$ μm (Al > 99.8 wt%), $d_{50}=12$ μm (Al > 99.5 wt%) and $d_{50}=2$ μm (Al > 99 wt%) were used in this study. The powders were gas atomized and collected under nitrogen. Electrolytic copper powder with the size of $d_{50}=45$ μm (Cu > 99.9 wt%) was used as the starting material for the Cu alloy element. Commercially available h-BN powder (1–5 μm particle size, 99 wt% pure) was used as the reinforcement in the as-forged composites.

2.2. h-BN/Al composite fabrication

Three different kinds of Al powders, electrolytic copper powder and h-BN powder were used to make Al-5.3 wt% Cu-3 wt% h-BN composite and Al-5.3 wt% Cu alloy samples. The powder mixtures were low energy ball milled using steel jars and balls (10 mm, 8 mm, and 4 mm diameter). N-hexane was used as the process control agent to avoid particles agglomeration. The milling was performed for 5 h with a ball-to-powder weight ratio of 4:1. The rotation speed of the steel vials was set at 200 rpm. After milling, the powders were naturally air dried. The powder mixture was pre-compacted under 5 MPa pressure in the high purity graphite mold, which was then heated in a furnace with high purity argon as the protective atmosphere. 10 MPa pressure was slowly applied at 640 ± 2 °C, and the pressure was held constant for 60 min. The pressure was then unloaded and the samples were cooled with the furnace. A schematic of the manufacturing process is illustrated in Fig. 1. Once the samples cooled down, sections were removed for analysis and the remainder of the composite samples was subjected to the T6 heat treatment within 48 h of forming. Along with the Al-5.3 wt% Cu without h-BN, the formed materials were solutionized at 537 ± 2 °C for 10 h, quenched in water at room temperature and immediately artificially aged at 175 ± 2 °C for 5 h. Different kinds of prepared samples A–F are summarized in Table 1.

Table 1
The samples from different starting powders prepared by the liquid phase forging.

Sample	Starting powder				
	Al ($d_{50}=35$ μm)	Al ($d_{50}=12$ μm)	Al ($d_{50}=2$ μm)	Cu	h-BN
A	■	–	–	■	–
B	■	–	–	■	■
C	–	■	–	■	–
D	–	■	–	■	■
E	–	–	■	■	–
F	–	–	■	■	■

2.3. Characterization

The powder morphology and bulk samples' microstructure were analyzed using scanning electron microscopy (SEM, LEO-1450). Energy dispersive spectrometry (EDS) was used to assist the SEM analysis. The interface between the h-BN and the Al matrix was carefully observed and analyzed using transmission electron microscopy (TEM, Tecnai G2 F30). Phase analysis of the composite and alloy samples was carried out by X-ray diffraction (XRD, Rigaku TTR III) using monochromatic Cu Kα radiation with the X-ray wavelength of 0.154 nm, operated at 40 kV and 150 mA. The hardness values of the samples were determined using the Brinell hardness tester (HB, DHB-3000, China) with 5 mm cemented carbide ball indenter, 2.5 kN load and the 30 s loading time. For each test, at least three specimens were tested to obtain the average hardness values. The standard deviation of the hardness measurements is 1.2 HB. The density of the as-forged materials was measured using the Archimedes' principle.

3. Results and discussion

3.1. Powders characterization

The representative morphology of the as-atomized Al powder and milled powder used in this work is shown in Fig. 2. Three

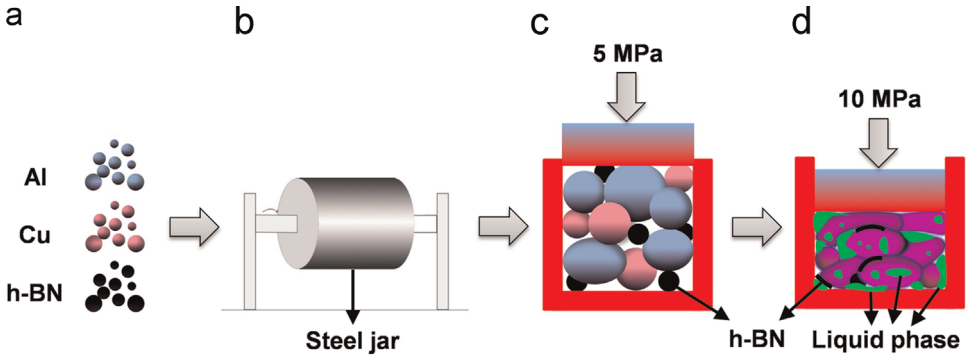

Fig. 1. Schematic drawing of the manufacturing process: (a) raw powders; (b) powder mixture by ball milling; (c) powder compact at room temperature under 5 MPa pressure; (d) densification of the powder compact at 640 °C under 10 MPa pressure.

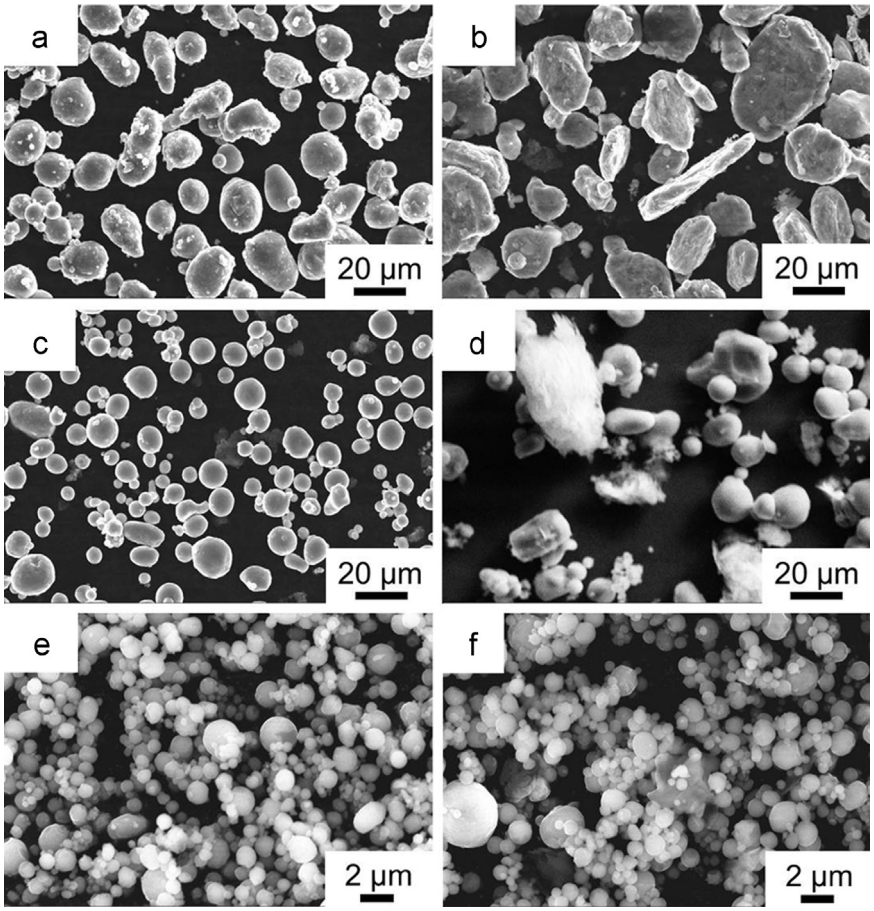

Fig. 2. SEM micrographs of Al powder with: (a) $d_{50}=35$ μm, (c) $d_{50}=12$ μm and (e) $d_{50}=2$ μm; Ball-milling powder with (b) $d_{50}=35$ μm, (d) $d_{50}=12$ μm and (f) $d_{50}=2$ μm Al powder.

different kinds of Al powder particles were primarily spherical. After milling, the $d_{50}=35$ μm Al powder particles were irregular and partially plate in shape, while the $d_{50}=2$ μm Al powder particles were still rounded. As for the $d_{50}=12$ μm Al powder, only a few particles got into the irregular shape and the remainder kept the roundness. This was because during milling, higher energy produced from the constant collision between the larger Al powder particles ($d_{50}=35$ μm) and the steel balls caused plastic deformation of the Al powder particles. In contrast, due to the lower collision energy of the smaller Al powder particles ($d_{50}=12$ and 2 μm), the plastic deformation was not easy to take place and the original powder morphology was preserved.

3.2. Densification behavior

Backscattered electron SEM observations shown in Fig. 4 reveal no apparent voids in the as-forged microstructure of the Samples B, D and F, which were almost fully dense Al matrix composites. The calculated theoretical density of Al – 5.3 wt% Cu and Al – 5.3 wt% – 3 wt% h-BN was 2.8 g cm^{-3} and 2.78 g cm^{-3}, respectively. The densities of the as-forged Al–Cu alloys and the h-BN/Al–Cu composites ranged from 98.9% to 99.6% of the theoretical density listed in Table 2. Fig. 3 clearly shows the different relative densities of the as-forged Al–Cu alloys and h-BN/Al–Cu composites with varying Al powder size. The improved density of the composites was closely related to the liquid phase formation, flow and filling the clearance between the solid grains in the semi-solid powder forging process. According to the binary phase diagram, the formation of Al-5.3 wt% Cu liquid phase started at approximately 548 °C. In this study, forging was performed at 640 °C,

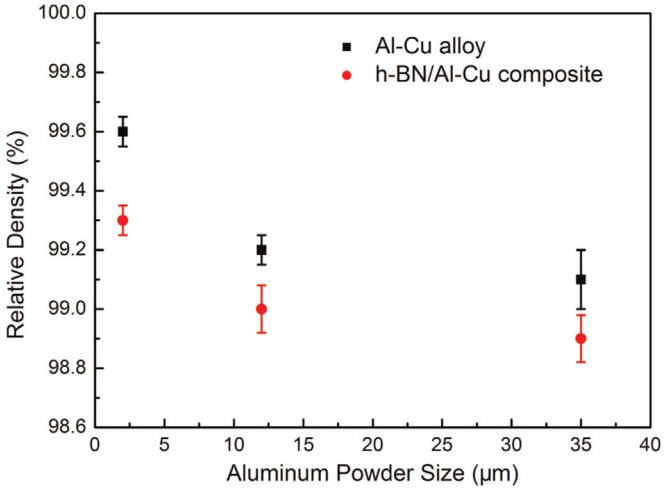

Fig. 3. Relative densities of the as-forged Al–Cu alloys and h-BN/Al–Cu composites with varying Al powder size.

which was about 100 °C above the liquid phase starting temperature when plenty of liquid phase existed in the material system. Under the action of capillary forces and loads, liquid phase flow accelerated and filled the pores, making the material denser. As shown in Fig. 3, the relative density of the alloy and the composite with the $d_{50}=2$ μm Al powder particles was higher than the alloy and the composite with the $d_{50}=35$ μm Al powder particles. Usually, the finer the powder particles, the larger the specific surface area and the intrinsic surface driving force. Due to

Table 2
Experimental density and relative density of the as-forged Al–Cu alloys and the h-BN/Al–Cu composites.

Sample	Theoretical density ($g\ cm^{-3}$)	Experimental density ($g\ cm^{-3}$)	Relative density (%)
A	2.8	2.78 ± 0.0028	99.1 ± 0.1
B	2.78	2.75 ± 0.0022	98.9 ± 0.08
C	2.8	2.78 ± 0.0014	99.2 ± 0.05
D	2.78	2.76 ± 0.0022	99.1 ± 0.08
E	2.8	2.79 ± 0.0014	99.6 ± 0.05
F	2.78	2.76 ± 0.0014	99.3 ± 0.05

abundant liquid phase, fine powder particles can easily rotate and move in the liquid phase, adjusting to the best filling position and improving the degree of densification. Compared with the Al–Cu alloy, the density of h-BN/Al–Cu composite prepared with the same Al powder was slightly lower. This indicated that h-BN could hinder densification to some extent. However, the applied loading can promote densification of the alloy and the composite by PM due to the abundance of the liquid phase.

The microstructure of the Samples B, D and F is notably different from one another, shown in Fig. 4. In Sample B synthesized with $d_{50}=35$ μm Al powder, grains in Fig. 4a were elongated perpendicular to the forging direction. Three reasons could account for this phenomenon. First, powder particles were in a softening state, greatly reducing the deformation resistance at the high experimental temperature of 640 °C. Plastic deformation of the powder particles took place easily under 10 MPa applied load, presenting as-forged texture morphology. Second, good h-BN lubrication at high temperature could reduce frictional resistance of particles rearrangement when deformation of the powder particles occurred. Last but not least, powder particles were milled into flakes, which remained in bulk composite microstructure. However, in the Samples D and F fabricated with $d_{50}=12$ and 2 μm Al powder, respectively, the grain deformation did not clearly occur in Fig. 4b and the grain morphology in Fig. 4c was not distinct due to the fine grains. In addition, white phases (marked as W in Fig. 4a) were intermittently distributed along the grain boundaries and inside the grains of the Sample B. Black phases (marked as R in Fig. 4a) with vermicular and flake shapes were located along the grain boundaries. The phases outlined above were observed to exist in the interior and at the interface of the undeformed grains in Fig. 4b. The white and black phases, denoted by W and R respectively in Fig. 4c, were also present in the Sample F, evenly distributed in the matrix, but partially agglomerated.

EDS analysis results are shown in Fig. 5. The white phases (marked as W) contained Al and Cu elements in Fig. 5a with 68.41 at% and 31.59 at% atomic percentages, respectively. The ratio of the atomic percentage of Al and Cu was nearly 2:1. Combined with the XRD patterns in Fig. 6, it was confirmed that the white W phase was Al_2Cu. As observed in Fig. 5b, the N element was found along with Al and Cu. It was noted that the atomic number of the boron element was rather low, resulting in difficulty of capturing its signal by EDS. While the size of the phase R was about 5 μm, the Al and Cu signals around the black phase were eventually collected in one minute. Moreover, a marginally visible h-BN peak identified to a (002) plane originated from dispersed 3 wt% h-BN can be seen at ~26.63° in Fig. 6a, c and e. Accordingly, it could be inferred that the black phase R labeled in Fig. 4 was h-BN. As for the gray phase G, only 1.26 at% Cu with over 98 at% Al appeared in Fig. 5c. Such a small amount of copper may be due to solid solution in the aluminum matrix, and the Al phase of six samples in Fig. 6 was well structured. Consequently, it was certain that the phase G was pure Al. These results proved that no other phases, like Al borides or nitrides had been formed in the h-BN/Al–Cu composites during the semi-solid powder forging.

Fig. 7 shows the microstructure of the samples B, D and F treated with the T6 condition. It can be clearly seen from Fig. 7a, d and g that with the decrease of Al powder size, the grain size became smaller. The grain boundary structures of the Samples B and D were optimized after the T6 heat treatment in Fig. 7a and d, compared with Fig. 4a and b, respectively. This resulted in continuous and uniform distribution of the Al_2Cu phase on the grain boundaries, clearly seen from Fig. 7b and e. High magnification SEM image in Fig. 7b shows retained deformation texture with one large elongated grain (~30 μm) and seven smaller 5–10 μm grains. This phenomenon was a result of the *in situ* recrystallization after the T6 heat treatment. Due to the pinning effect of the secondary phase particles (Al_2Cu, h-BN) and Al powder surface oxide particles, the subgrain boundary formed in the forging process could not move, and was also unable to break through the

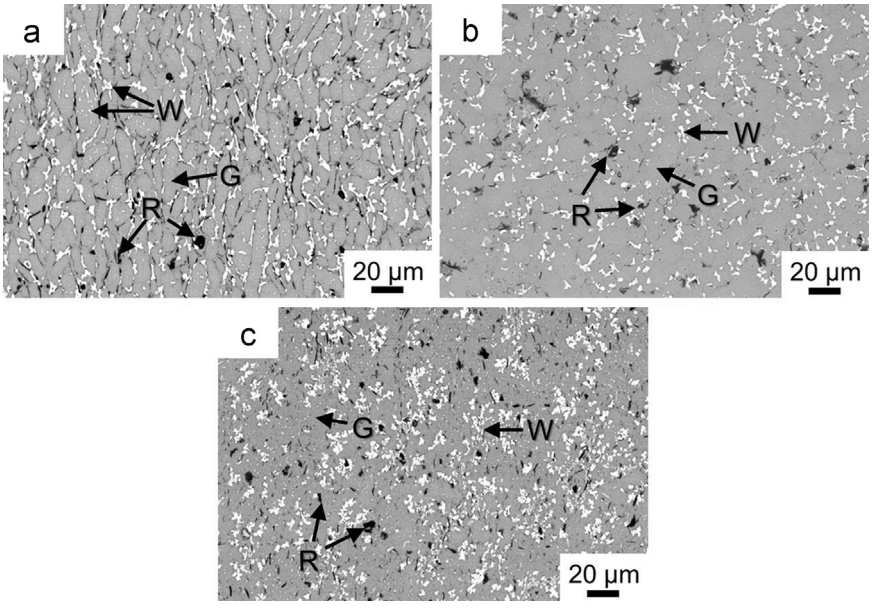

Fig. 4. Backscatter SEM micrographs of the as-forged h-BN/Al–Cu composites with different Al powders: (a) $d_{50}=35$ μm, (b) $d_{50}=12$ μm and (c) $d_{50}=2$ μm. The alphabetic characters, W, R and G, represent the white, black and gray phase, respectively.

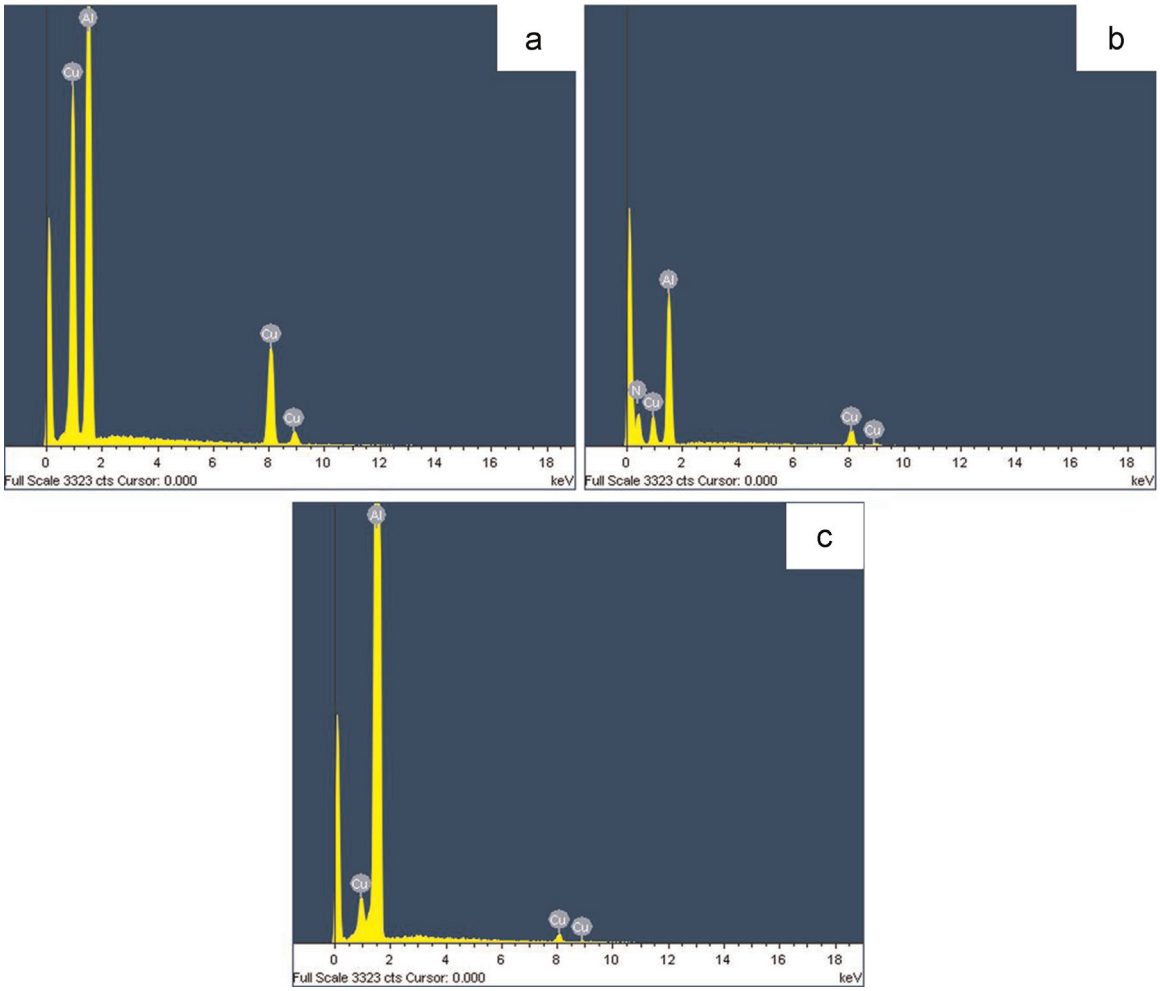

Fig. 5. EDS spectra of: (a) point *W*; (b) point *R* and (c) point G in Fig. 4.

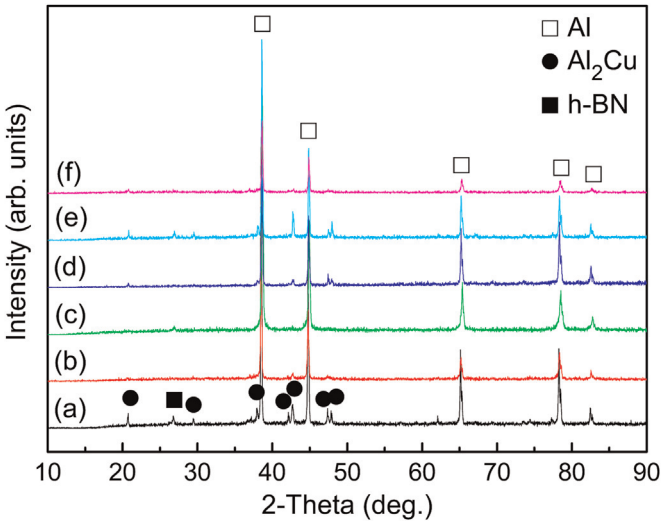

Fig. 6. XRD patterns of h-BN/Al–Cu composites of the as-forged (a, c and e) and after T6 heat treatment (b, d and f) with different Al powders: (a and b) d_{50}=35 μm, (c and d) d_{50}=12 μm and (e and f) d_{50}=2 μm.

bondage of the master grain boundary. Dislocations continued to be absorbed, and dislocation tangles were gradually eliminated. As a result, grain misorientation increased gradually, and finally low angle grain boundaries (LAGBs) transformed into high angle grain boundaries (HAGBs), leading to the transformation from the subgrains to true grains. Eventually, several small grains formed inside the master grain through the segmentation of the master grain in the form of subgrains aggregation and coarsening [20]. Compared with the microstructure in Fig. 4c, smaller 1–2 μm Al_2Cu particles were distributed evenly in the matrix of the Sample F after T6 heat treatment, as shown in Fig. 7i.

3.3. Interface

To ascertain the effect of semi-solid powder forging on the status of the interface bonding between the h-BN and the Al matrix, TEM analysis was carried out with the Samples B and F after solid solution treatment. Secondary phases, for instance, the Al_2Cu phase, can be fully dissolved in the matrix with the reasonable solid solution treatment to facilitate observations of the interface characteristics between the h-BN and the Al matrix. In Fig. 8, bright field TEM images of the as-forged material and high resolution TEM (HRTEM) images of the h-BN and Al matrix interface are shown. As indicated in Fig. 8a and c, a sharp interface consisting of Al/Al_2O_3/h-BN was present in the two composites. The thickness of the surface oxides of the Sample F prepared with d_{50}=2 μm Al powder particles was larger than the Sample B prepared with the d_{50}=35 μm Al powder particles. As measured in Fig. 8b and d, the former was about 20 nm, while the latter was just 2 nm. This suggested that the content of the surface oxides was higher in the d_{50}=2 μm Al powder particles than in the d_{50} =35 μm Al powder particles, which agreed with the Al powder purity in the starting materials.

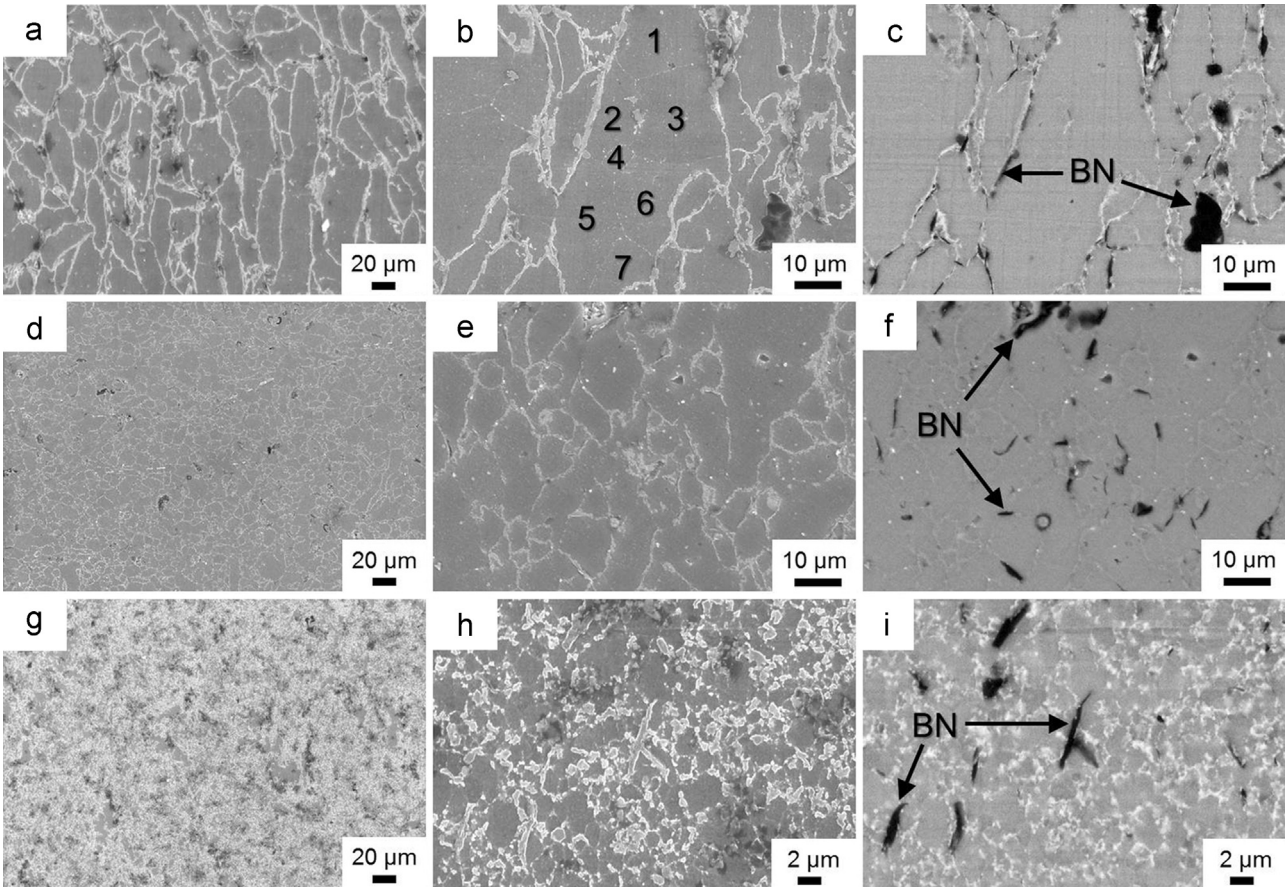

Fig. 7. SEM micrographs of the h-BN/Al–Cu composites with different Al powders after the T6 heat treatment: (a and b) $d_{50}=35$ μm, (d and e) $d_{50}=12$ μm and (g and h) $d_{50}=2$ μm. The images (c), (f) and (i) are backscattered electron micrographs corresponding to (b), (e) and (h), respectively.

Based on the previous research [18], in the h-BN reinforced composites, AlN and AlB_2 phases were not formed by the direct reaction at the interface between the h-BN and the Al matrix. This interesting finding was also confirmed by the XRD results of the composite in Fig. 6. It was considered that the original Al_2O_3 skin was introduced naturally in the surface of the Al powder particles, hindering the interfacial reaction between Al and h-BN in the process of powder liquid phase forging. On the other hand, the experimental temperature was not high enough to allow the reaction between Al_2O_3 and h-BN to occur. Nevertheless, h-BN was closely combined with the Al matrix through the Al_2O_3 layer, and there was no gap between the interfaces.

In addition, the HRTEM image depicted in Fig. 8b shows the lattice fringes of individual h-BN. Characteristic (002) fringes separated by a 0.33 nm distance, peculiar to a Van-der-Waals spacing in h-BN were particularly visible. Similarly, our results notably agreed with the recent report by Yamaguchi et al. [21].

TEM selected area diffraction patterns (SADP) of the Al matrix and the reinforced h-BN phase of the Samples B and F after solid solution treatment are shown in Fig. 9a and b, along the SEM micrographs and XRD patterns of the h-BN powder, shown in Fig. 9c and d, respectively. The Al matrix showed single crystal diffraction spots, and h-BN had characteristic polycrystalline diffraction rings. As seen in Figs. 7 and 8, h-BN powder particles in Fig. 9c presented the flake structure with 1–5 μm diameter and 0.2–0.5 μm thickness. In the XRD spectrum shown in Fig. 9d, three diffraction peaks with the (002), (100) and (110) crystal planes were clearly observed in agreement with the SADP results in Fig. 9b.

3.4. Hardness measurements

The Brinell hardness values of the investigated samples A–F in the as-forged, solution treated and aged conditions are presented in Fig. 10. For the same sample type, the hardness after solution and aged treatments was higher than the as-forged as a result of solution strengthening and age hardening, respectively. Comparing the Al–Cu alloy with the corresponding h-BN/Al–Cu composite under the T6 treatment, the hardness of the composite was increased by 17%, 12.6% and 14.3% with $d_{50}=35$, 12 and 2 μm Al powder, respectively, due to the addition of the h-BN powder particles. It was indicated that despite the significantly low content (3 wt%) of the h-BN powder particles in the composite, its influence on the macroscopic mechanical properties of the material was prominent. Also, it was reflected that the densification degree of the h-BN reinforced Al matrix composite by the semi-solid powder forging was very high, since lower density (higher porosity) must cause lower material hardness.

Moreover, as for the composites fabricated using Al powders with different granularity, the hardness under the same treatment was largely affected, increasing with the decrease of the Al powder size. For instance, the hardness of the composite with the $d_{50}=2$ μm Al powder particles was 16.4% higher than the $d_{50}=35$ μm Al powder particles under the T6 treatment. The hardness increase in the composite with the $d_{50}=2$ μm Al powder particles may come from three main contributors. First, as shown in material microstructure, fine Al_2Cu and h-BN particles were evenly distributed in the Sample F matrix, while the two phases were mainly along the grain boundaries of the Sample B. Second, the surface oxides of the fine Al powder were thicker than the coarse Al

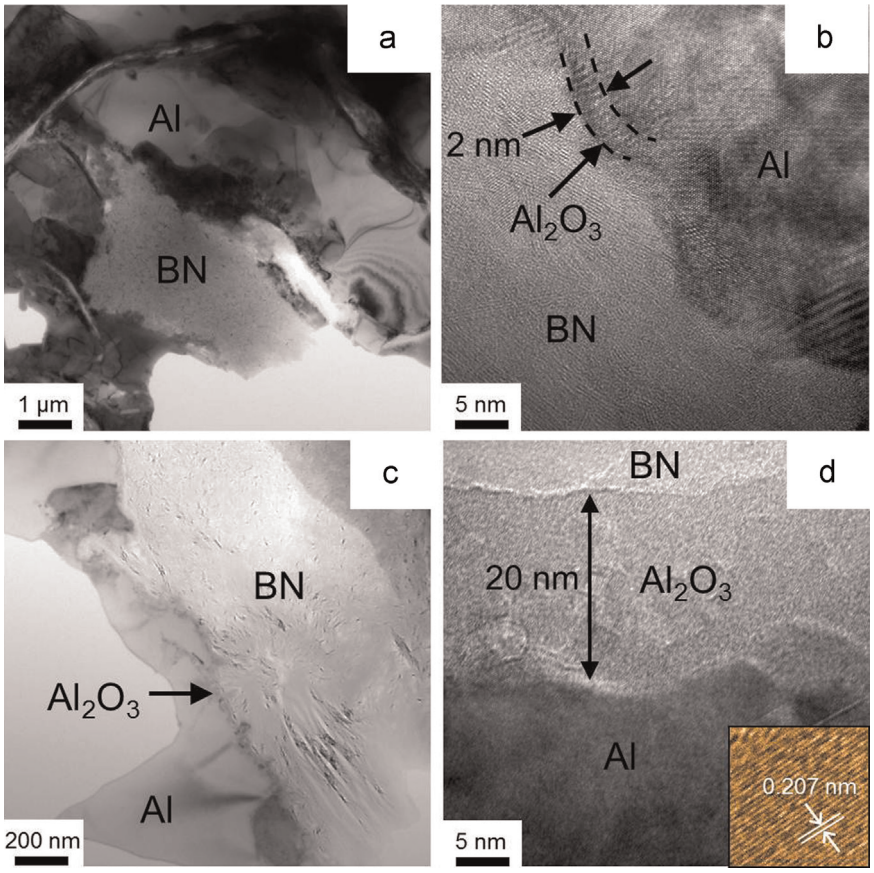

Fig. 8. TEM and HRTEM micrographs of h-BN/Al–Cu composites with (a and b) d_{50}=35 μm Al powder and (c and d) d_{50}=2 μm Al powder after solid solution treatment. A sharp interface between the h-BN and the Al matrix is present. The bottom right corner in (d) is the corresponding lattice fringe image from the Al_2O_3 nanolayer.

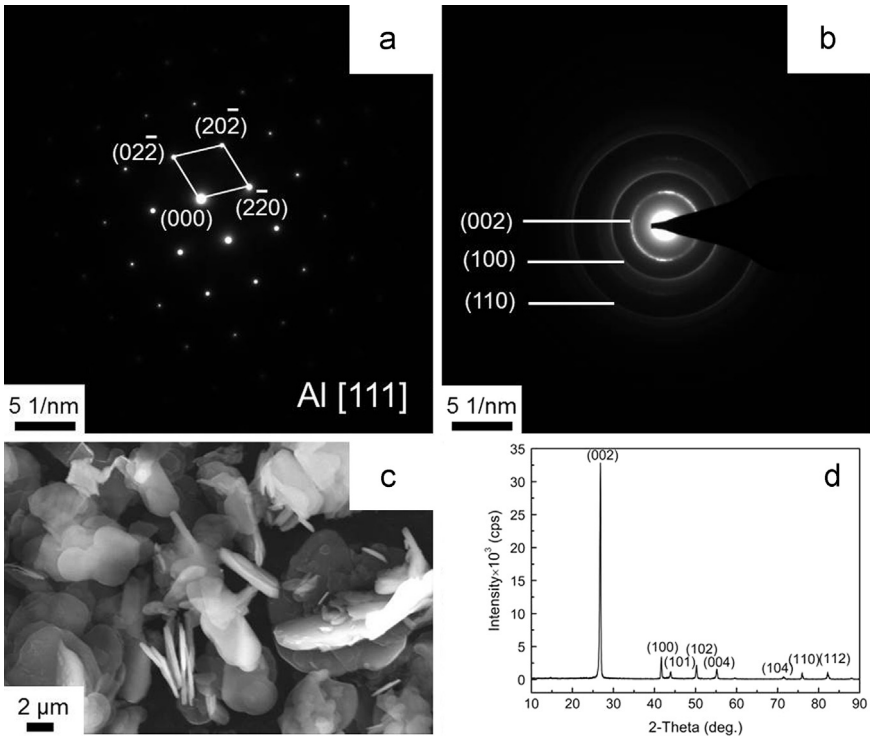

Fig. 9. The SADP of: (a) the Al matrix and (b) h-BN of the h-BN/Al–Cu composite; (c) SEM micrograph and (d) XRD patterns of the h-BN powder.

powder because the Al_2O_3 content of the Sample F was higher than the Sample B. As a ceramic phase, Al_2O_3 could contribute to the improved hardness. Besides, the grains prepared with fine Al powder were smaller, as seen in Fig. 7h. It could be deduced that the increased hardness was related to the grain refinement strengthening.

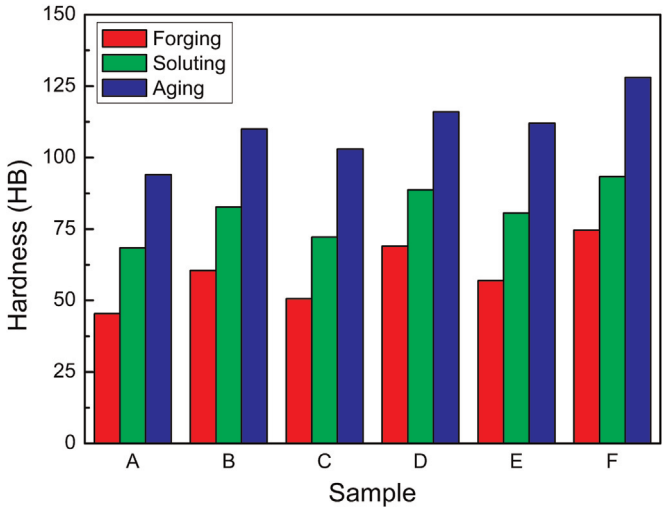

Fig. 10. Hardness variation of the samples with different treatment.

3.5. Compressive behavior

The compressive strength values of the investigated composites after T6 treatment, shown in Fig. 11 and Table 3 increased with the decrease of the Al powder size. It was 525 MPa, 560 MPa and 763 MPa for the T6 specimens prepared with d_{50}=35, 12 and 2 μm Al powder, respectively. Likewise, the strain at which failure of the T6 specimens occurred were inversely proportional to the size of Al powder, seen in Fig. 11, where, it was 0.063, 0.127 and 0.299, corresponding to d_{50}=35, 12 and 2 μm Al powder, respectively. In some works [22–25], it has been reported that some of the important factors responsible for enhancing the mechanical properties were the grain size, necessary dislocations and Orowan's strengthening. In general, composite strength is improved by the addition of solid particles dispersed in the matrix material. In this study, the addition of h-BN in three kinds of composites was consistent with one another. Thus, the content of the h-BN particles was not the main reason for improving composite strength. Nevertheless, the stronger the contact between the matrix and reinforcement particles, the lower the probability of crack initiation and propagation [19]. As presented above, a sharp interface without pores between the matrix and reinforcement assured effective load transfer from the alloy matrix and the reinforcement.

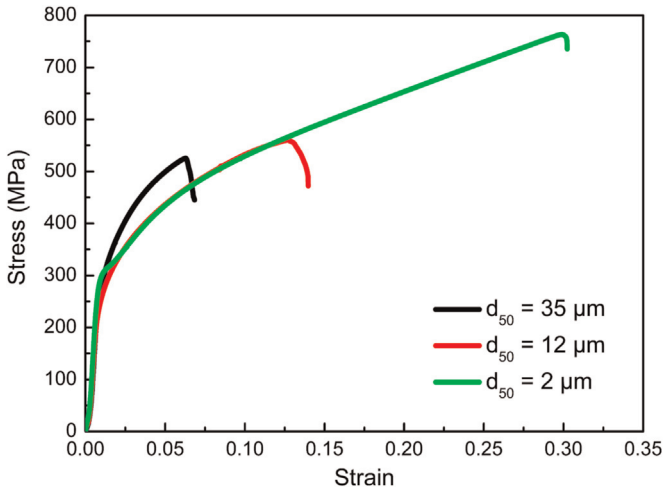

Fig. 11. Compressive stress–strain curves of the h-BN/Al–Cu composites synthesized with d_{50}=35, 12 and 2 μm Al powder.

Table 3
Compressive strength and its reflected fracture strain of the h-BN/Al–Cu composites after T6 heat treatment.

Al powder size d_{50} (μm)	Compressive strength (MPa)	Fracture strain
35	525 ± 3	0.063 ± 0.002
12	560 ± 3	0.127 ± 0.002
2	763 ± 3	0.299 ± 0.002

The Al_2Cu particles which were the primary precipitates in the Al–Cu alloy series played a major role in improving the mechanical properties. It was discovered that the h-BN/Al–Cu composite with d_{50}=2 μm Al powder showed significantly enhanced mechanical properties. The remarkable increase in both compressive strength and fracture strain can be due to substantial grain refinement and the presence of reasonably distributed hard particulates (nano-Al_2O_3) and intermetallic phases (Al_2Cu) in the matrix, which can be strongly backed up by the microstructure in Figs. 7 and 8. It should be noted that the optimal fracture strain was the consequence of the increase in fracture strain attributed to grain refinement superior to the reduction effect caused by the secondary phase particles. In addition, as illustrated in Fig. 3, high relative density of the composite prepared with the d_{50}=2 μm Al powder may enhance its compressive properties further.

Overall, the h-BN/Al–Cu composite with the d_{50}=2 μm Al powder by the semi-solid powder forging showed the best mechanical performance, including the Brinell hardness, compressive strength and fracture strain. The results of this study clearly illustrated the capability of the h-BN/Al composite with ultrafine Al powder by the semi-solid powder forging to exhibit superior mechanical properties, making the technique a potential process for structural and functional materials in weight critical engineering applications.

4. Conclusions

The following conclusions can be made from the present study:

(1) Al-5.3 wt% Cu composite reinforced by 3 wt% h-BN with nearly full densification was successfully fabricated by the semi-solid powder forging process. The densification mechanism was due to the action of capillary forces and applied loading, where abundant accelerated liquid phase flow filled the pores, making the material ultimately denser.

(2) The h-BN/Al-Cu composites prepared using Al powder with varying granularity showed different microstructures, such as grain characteristics, the morphology and distribution of h-BN powder particles and the Al_2Cu phase. *In situ* recrystallization occurred inside the original grains with d_{50}=35 μm Al powder.

(3) A sharp interface consisting of Al/Al_2O_3/h-BN was present in the composites fabricated by the semi-solid powder forging. The thickness of the surface oxides of d_{50}=2 μm Al powder particles was about 20 nm, while that of d_{50}=35 μm Al powder particles was just 2 nm.

(4) Due to the high relative density, significant grain refinement and the presence of reasonably distributed hard particulates (nano-Al_2O_3) and intermetallic phases (Al_2Cu) in the matrix, the h-BN/Al–Cu composite with the d_{50}=2 μm Al powder by the semi-solid powder forging showed the best mechanical performance, including the Brinell hardness, compressive strength and fracture strain.

Acknowledgments

This work was supported by the National High Technology Research and Development Program of China (863 Program, No. 2013AA031104).

References

[1] M.D. Harding, I.W. Donaldson, R.L. Hexemer Jr., M.A. Gharghouri, D.P. Bishop, Characterization of the microstructure, mechanical properties, and shot peening response of an industry processed Al–Zn–Mg–Cu PM alloy, J. Mater. Process. Technol. 221 (2015) 31–39.
[2] N. Guo, B. Luan, F. He, Z. Li, Q. Liu, Influence of flake thickness on the shape and distribution of Al_2O_3 particles in Al matrix composites fabricated by flake powder metallurgy, Scr. Mater. 78–79 (2014) 1–4.
[3] C.G. Chen, J. Luo, Z.M. Guo, W.W. Yang, J. Chen, Microstructural evolution and mechanical properties of *in situ* TiB_2/Al composites under high-intensity ultrasound, Rare Met. 34 (2015) 168–172.
[4] M. Balog, P. Krizik, M. Yan, F. Simancik, G.B. Schaffer, M. Qian, SAP-like ultrafine-grained Al composites dispersion strengthened with nanometric AlN, Mater. Sci. Eng. A 588 (2013) 181–187.
[5] W.W. Yang, Z.M. Guo, L.C. Guo, H.Q. Cao, J. Luo, A.P. Ye, *In situ* fabrication and properties of AlN dispersion strengthened 2024 aluminum alloy, Int. J. Miner. Metall. Mater. 21 (2014) 1228–1232.
[6] M. Balog, C. Poletti, F. Simancik, M. Walcher, W. Rajner, The effect of native Al_2O_3 skin disruption on properties of fine Al powder compacts, J. Alloy. Compd. 509S (2011) S235–S238.
[7] M. Balog, F. Simancik, M. Walcher, W. Rajner, C. Poletti, Extruded Al–Al_2O_3 composites formed in situ during consolidation of ultrafine Al powders: effect of the powder surface area, Mater. Sci. Eng. A 529 (2011) 131–137.
[8] M. Balog, P. Krizik, M. Nosko, Z. Hajovska, M.V.C. Riglos, W. Rajner, D.S. Liu, F. Simancik, Forged HITEMAL: Al-based MMCs strengthened with nanometric thick Al_2O_3 skeleton, Mater. Sci. Eng. A 613 (2014) 82–90.
[9] X. Luo, Y. Liu, C. Gu, Z. Li, Study on the progress of solidification, deformation and densification during semi-solid powder rolling, Powder Technol. 261 (2014) 161–169.
[10] Y. Wu, G.Y. Kim, Compaction behaviour of Al6061 powder in the semi-solid state, Powder Technol. 214 (2011) 252–258.
[11] C.E. Wen, Fabrication of TiAl by blended elemental powder semisolid forming, J. Mater. Sci. 36 (2001) 1741–1745.
[12] Y. Wu, G.Y. Kim, I.E. Anderson, T.A. Lograsso, Fabrication of Al6061 composite with high SiC particle loading by semi-solid powder processing, Acta Mater. 58 (2010) 4398–4405.
[13] Y. Wu, G.Y. Kim, Carbon nanotube reinforced aluminum composite fabricated by semi-solid powder processing, J. Mater. Process. Technol. 211 (2011) 1341–1347.
[14] B. Podgornik, T. Kosec, A. Kocijan, Č. Donik, Tribological behaviour and lubrication performance of hexagonal boron nitride (h-BN) as a replacement for graphite in aluminium forming, Tribol. Int. 81 (2015) 267–275.
[15] Z.P. Xia, Z.Q. Li, C.J. Lu, B. Zhang, Y. Zhou, Structural evolution of Al/BN mixture during mechanical alloy, J. Alloy. Compd. 399 (2005) 139–143.
[16] Q. Peng, W. Ji, S. De, Mechanical properties of the hexagonal boron nitride monolayer: *ab initio* study, Comput. Mater. Sci. 56 (2012) 11–17.
[17] Y.T. Zheng, H.B. Li, T. Zhou, Microstructure and mechanical properties of h-BN—SiC ceramic composites prepared by in situ combustion synthesis, Mater. Sci. Eng. A 540 (2012) 102–106.
[18] K.B. Lee, H.S. Sim, S.W. Heo, H.R. Yoo, S.Y. Cho, H. Kwon, Tensile properties and microstructures of Al composite reinforced with BN particles, Compos. Part A 33 (2002) 709–715.
[19] O.A.M. Elkady, A. Abu-Oqail, E.M.M. Ewais, M. El-Sheikh, Physico-mechanical and tribological properties of Cu/h-BN nanocomposites synthesized by PM route, J. Alloy. Compd. 625 (2015) 309–317.
[20] H. Jazaeri, F.J. Humphreys, The transition from discontinuous to continuous recrystallization in some aluminium alloys II – annealing behaviour, Acta Mater. 52 (2004) 3251–3262.
[21] M. Yamaguchi, F. Meng, K. Firestein, K. Tsuchiya, D. Golberg, Powder metallurgy routes toward aluminum boron nitride nanotube composites, their morphologies, structures and mechanical properties, Mater. Sci. Eng. A 604 (2014) 9–17.
[22] C. Yang, Y. Zong, Z. Zheng, D. Shan, Experimental and theoretical investigation on the compressive behaviour of aluminum borate whisker reinforced 2024Al composites, Mater. Charact. 96 (2014) 84–92.
[23] M.K. Habibi, M. Qian, A.S. Hamouda, M. Gupta, Differentiating the mechanical response of hierarchical magnesium nano-composites as a function of temperature, Mater. Des. 42 (2012) 102–110.
[24] Q.B. Nguyen, M. Gupta, Enhancing compressive response of AZ31B using nano-Al_2O_3 and copper additions, J. Alloy. Compd. 490 (2010) 382–387.
[25] R. Anish, M. Sivapragash, G. Robertsingh, Compressive behaviour of SiC/ncsc reinforced Mg composite processed through powder metallurgy route, Mater. Des. 63 (2014) 384–388.